Spin-glass behavior and vacancy order in van der Waals layered β-MoCl_{4}

Michael A. McGuire and Brian C. Sales

Phys. Rev. Materials **2**, 074007 — Published 30 July 2018

DOI: 10.1103/PhysRevMaterials.2.074007

Spin-glass behavior and vacancy order in van der Waals layered β-$MoCl_4$

Michael A. McGuire[1,*] and Brian C. Sales[1]

[1]*Materials Science and Technology Division, Oak Ridge National Laboratory, Oak Ridge, Tennessee 37831 USA*

Two-dimensional β-$MoCl_4$ is an attractive material from the perspectives of magnetism in $4d$ transition metal compounds, geometrically frustrated lattices, and magnetic van der Waals layered materials, but the magnetism in this compound has not been particularly well studied to date. Here the magnetic properties and crystal structure of $MoCl_4$ are revisited, and results of ac and dc magnetic measurements and single crystal x-ray diffraction are reported. Crystals grow as well-formed and easily cleaved hexagonal plates that are unstable in air. The revised structural model comprises $CdCl_2$-type layers with 50% Mo vacancies distributed over the sites of the triangular cation net. Interestingly, a structural ambiguity regarding the vacancy distribution is identified in the analysis of the diffraction data. The orbital moment is not expected to be quenched in this $4d^2$ compound. Accordingly, magnetization measurements indicate an effective moment that is about 20% lower than the spin-only value. The magnetic data reveal an anomaly near 5 K, below which a divergence of field-cooled and zero-field-cooled dc magnetization, a slow relaxation of thermo-remanent magnetization, and enhanced frequency dependence of ac magnetization are observed. Thus, β-$MoCl_4$ represents an uncommon example of a cleavable spin-glass system.

I. INTRODUCTION

There is ongoing interest in van der Waals bonded low dimensional magnetic materials, as well as magnetism in $4d$ transition metal compounds with extended d-orbitals and significant spin-orbit coupling. Cleavable and monolayer magnetic materials can be produced from van der Waals layered compounds, enabling the investigation of novel physics and heterostructured devices[1] in materials like CrI_3[2–5], $CrGeTe_3$[6–9], and Fe_3GeTe_2[10–13]. While such materials rely primarily on $3d$ transition metal magnetism, extending into $4d$ and $5d$ elements is of interest because of the increased extension of the d-orbitals and more covalent bonding, which has the potential to lead to stronger magnetic interactions, and more significant spin-orbit coupling strength[14–21].

Transition metal halides provide a chemically versatile family of layered materials incorporating $3d$, $4d$, and $5d$ elements[22], in particular binary dihaldes and trihalides, which adopt structures with triangular or honeycomb 2D sheets of transition metals. Based on progress made with the cleavable ferromagnet CrI_3[2–5] isoelectronic Mo is an interesting candidate for further study. MoF_3 has a relatively high antiferromagnetic ordering temperature of 185 K[23], more than twice as high as the analogous $3d$ compound CrF_3 (70 K[24,25]). While the fluorides do not have layered structures, molybdenum trichloride does. $MoCl_3$ was found to undergo a magnetostructural phase transition near 580 K, below which the magnetic moments are quenched by a distortion of the honeycomb net that results in Mo−Mo dimerization[26–28]. The magnetic susceptibility at high temperatures suggested strong magnetic correlations in the undimerized state, and support for this was provided by first principles calculations[26]. In an effort to unlock the expected strong magnetism in this phase, we have been exploring chemical modifications of the $MoCl_3$ structure aimed at destabilizing the dimer state. This led to our current study of $MoCl_4$, which is known to have a structure similar to $MoCl_3$. Here we have reexamined the structural and magnetic properties of this material.

There are two reported polymorphs of $MoCl_4$. The α-$MoCl_4$ polymorph has a 1D chain structure with a reduced magnetic moment due to partial dimerization, and a transition to a non-magnetic state under pressure has been recently predicted[29–31]. β-$MoCl_4$ is known to adopt a van der Waals layered structure related to those common in dihalides and trihalides[22], with Mo atoms occupying a subset of sites on a triangular lattice of octahedral holes between two close-packed Cl layers. The composition can be descriptively written as $Mo_{0.75}Cl_3$. Both a fully disordered honeycomb model[27] and a fully ordered hexamer model[32] have been proposed for the Mo sublattice. Schäfer and von Schnering tabulated magnetization values at room temperature, 195 K, and 90 K from measurements on two specimens and from previous literature, and the data indicated paramagnetic behavior with moments reduced from the expected value for S = 1, and antiferromagnetic interactions[27]. No more recent or more complete investigations were found in the literature.

In the present work, the crystal structure of layered β-$MoCl_4$ has been redetermined by single crystal x-ray diffraction, and its magnetic behavior has been measured down to 2 K. The structure determined is a variation of that reported in Ref. 27 with additional disorder in the Mo sublattice. In addition, an interesting crystallographic ambiguity is noted, with two vacancy ordering models that are essentially indistinguishable by diffraction. Magnetic measurements on single crystal and polycrystalline material reveal an anomaly near 5 K, and behavior suggestive of glassy spin dynamics. The effective moment is found to be about 20% lower than the expected value for $S = 1$, indicating the presence of an unquenched orbital moment antialigned with the spin moment, which may be expected in this $4d^2$ compound.

Due to its layered structure, chemical disorder, and antiferromagnetic interactions, β-$MoCl_4$ is a cleavable spin-glass. Development of such materials may enable the study of glassy spin systems in the 2D limit and integration of metastable and dynamic magnetism in van der Waals heterostructures.

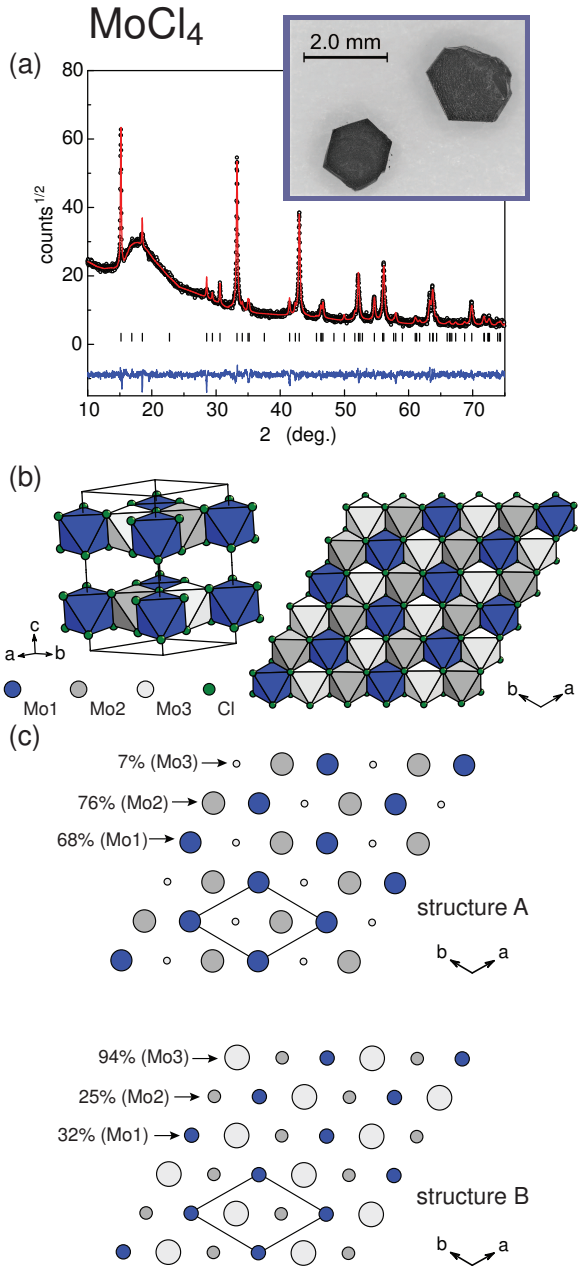

FIG. 1. (a) Crystals of $MoCl_4$ under paratone oil, and a Lebail fit to powder x-ray diffraction data using the structure determined by single crystal diffraction. (b) The layered crystal structure of the $MoCl_4$, with the octahedra around the partially occupied Mo sites shown in dark blue (Mo1), medium grey (Mo2), and light grey (Mo3), and with chlorine atoms in green. (c) The Mo layers in structure models A and B shown with areas proportional to the refined occupancies with corresponding labels. See text for details.

II. METHODS

Crystals of $MoCl_4$ were grown by reacting $MoCl_5$ (Alfa Aesar, 99.6% metals basis) with Mo powder (Alfa Aesar, 99.999% metals basis) inside evacuated, sealed, silica ampoules. The Mo powder was first reduced in a flowing mixture of argon and hydrogen (96:4) at 1000°C overnight. The $MoCl_5$ was used as received (packed under argon) and opened in the glovebox. Both $MoCl_4$ and $MoCl_5$ are very air sensitive. The starting materials were loaded into silica tubes inside the glovebox and transferred without exposure to air to a vacuum line for flame sealing. The sealed ampoules were placed in a horizontal tube furnace and the open ends were plugged with fiber insulation. The tube was positioned so the starting materials were at the end near the furnace opening and the empty end of the tube was near the thermocouple used for temperature control at the center. A natural temperature gradient exists in the furnace. The furnace was set so that the end of the ampoule near the center of the furnace was at 250°C, and once equilibrated the other end of the ampoule, where the reaction charge was located, was near 230°C as measured by an additional thermocouple. The reaction as left under these conditions for one to several days. Performing this reaction with a stoichiometric mixture of Mo and $MoCl_5$ (1:4) produced a black product containing small (sub-milimeter) hexagonal platelets, determined as described below to be $MoCl_4$. Performing the same reaction with an excess of Mo (1:1) produced a similar black product containing larger platelets, like those shown in Figure 1a, along with residual, unreacted Mo powder. When heated to a higher temperature, 350°C, the 1:1 loading produced Mo plus a red crystalline product determined to be $MoCl_3$.

For single crystal x-ray diffraction measurements crystals were covered in Paratone oil before removal from the glovebox and then mounted on a Bruker APEX diffractometer (Mo Kα radiation). Full hemispheres of data were collected on a platelet of $MoCl_4$. Data were reduced using SAINTPlus, with empirical absorption corrections applied using SADABS and space group identification and further data preparation carried out using XPREP. The structure was refined using ShelXL[33] within WinGX[34]. Powder x-ray diffraction data was collected using a PANalytical X'Pert Pro MPD with a dome-style air sensitive sample holder made by Anton Paar. Energy dispersive spectroscopy (EDS) data was collected using a Bruker Quantax70 detector and a Hitachi TM3000 scanning electron microscope. Samples were mounted on carbon tape and covered with Kapton film in the glovebox, then brought out, uncovered, and quickly inserted into the SEM antechamber to minimize air exposure. For magnetization measurements samples were loaded in the glovebox into 2 mm inner diameter silica tubes with 0.5 mm thick walls and sealed under helium; the measurements were performed using a Magnetic Property Measurement System SQUID magnetometer (Quantum Design).

III. RESULTS AND DISCUSSION

A. Crystal structure

Indexing single crystal diffraction data from small hexagonal plates of $MoCl_4$ gave a hexagonal unit cell with $a = 6.04$ Å and $c = 12.64$ Å. This is incompatible with the previously

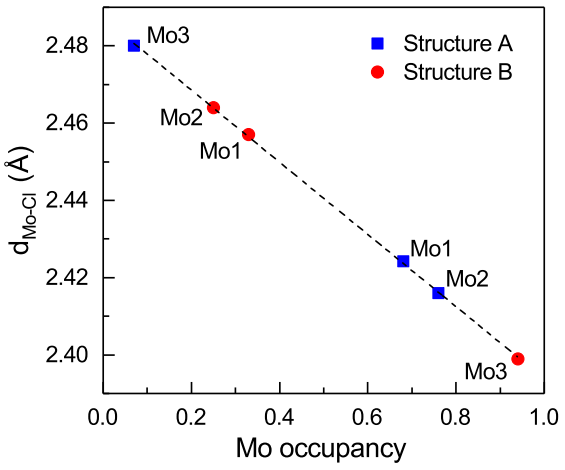

FIG. 2. Distances between Mo and coordinating Cl ions in the two structural models for $MoCl_4$ as a function of the corresponding Mo site occupancy.

reported hexamer structure, which has only one layer per cell and a correspondingly shorter *c*-axis[32], but is similar to the cell for the previously reported disordered-honeycomb structure[27]. Refinement of the data using that structure (space group $P\overline{3}1c$) as a starting model gave an R_1 value for all data of about 0.10, a relatively large difference peak at the centers of the honeycomb cells ($9\,e^-\mathring{A}^{-3}$), and a stoichiometry of $Mo_{2.88}Cl_{12}$. Including a partially occupied Mo site at the position of the large difference peak gave $R_1 = 0.048$ for all data, a largest difference peak less than $1\,e^-\mathring{A}^{-3}$ and a stoichiometry of $Mo_{3.03}Cl_{12}$. The occupancy of the central Mo site, Mo3, refined to 7%, while the occupancy of the two Mo sites forming the honeycomb net, Mo1 and Mo2, refined to 68 and 76%, respectively. This structure is referred to below as structure A.

Interestingly, another configuration was found that corresponds to a different vacancy distribution in the Mo layer that gave a nearly identical fit to the observed data. This second model contains a single nearly fully occupied Mo site (Mo3) surrounded by a honeycomb net of relatively low occupancy. In this case, the occupancy of Mo3 refined to 94%, while the Mo1 and Mo2 sites had occupancy of 32 and 25%, respectively. Like structure A, this corresponds to a stoichiometry of $Mo_{3.03}Cl_{12}$. This structure is referred to below as structure B. Refinement results for the two structural models are compared in Table I, with atomic displacement parameters given in Table II. Figure 1c compares the Mo layers in structures A and B, with the Mo sites represented so that their relative areas in the plane correspond to their occupancies.

The structures are shown in Figure 1b, and are composed of layers similar to those found in the $CdCl_2$ and CdI_2 structure types. Each Mo site is in edge sharing octahedral coordination by Cl ions, forming a triangular net within the *ab*-plane. The three Mo sites each form triangular lattices that interpenetrate to form the close-packed Mo sublattice. In structure A, the darkest octahedra are nearly vacant while the medium and light octahedra are mostly occupied, forming the honeycomb lattice. In structure B, the darkest octahedra are nearly fully occupied, forming a triangular lattice, and the medium and light octahedra are mostly vacant. The in-plane nearest neighbor Mo-Mo distance is 3.49 Å, and the distance along c between the Mo layers is 5.82 Å.

While structure B gives slightly better values than structure A for the goodness of fit, weighted R values, and difference peaks and holes, the differences are small. The atomic displacement parameters also do not provide definitive preference for one structure over the other (Tables I and II). Reasonable values for all atoms are seen in both structures. The smaller value for Mo3 in structure A is notable, but this site is only about 7% occupied. The vacancy distribution in structure B has a slightly higher configurational entropy than that in structure A, which may indicate the former to be more stable. Thus, it appears that the diffraction data cannot be used to distinguish clearly between structures A and B, with B being perhaps negligibly preferred.

To explore this apparent coincidence further, structure factor calculations were performed using both Platon and Mathematica for a simple model that includes only partially occupied Mo sites at the three positions that make up the Mo triangular net in these structures (Cl atoms excluded). It was found that for any such lattice with site occupancies of $\mathcal{O}_1$, $\mathcal{O}_2$, and $\mathcal{O}_3$ for Mo1, Mo2, and Mo3, respectively, an indistinguishable diffraction pattern is produced by a lattice with occupancies $1-\mathcal{O}_1$, $1-\mathcal{O}_2$, and $1-\mathcal{O}_3$, provided $\mathcal{O}_1+\mathcal{O}_2+\mathcal{O}_3 = \frac{3}{2}$, or equivalently that the average occupation of the three sites is one half. These relationships are approximately obeyed by the occupancy parameters for Structures A and B listed in Table I and represented in Figure 1c. More generally, if $\mathcal{O}_1+\mathcal{O}_2+\mathcal{O}_3 = \mathcal{O}_{tot}$, then $\mathcal{O}_1$, $\mathcal{O}_2$, and $\mathcal{O}_3$ gives the same diffraction as $\frac{2}{3}\mathcal{O}_{tot}-\mathcal{O}_1$, $\frac{2}{3}\mathcal{O}_{tot}-\mathcal{O}_2$, and $\frac{2}{3}\mathcal{O}_{tot}-\mathcal{O}_3$. This was confirmed empirically using Platon with several sets of occupancy numbers. It is expected that this is a geometrical property of this particular lattice, though the equivalence is difficult to show analytically.

The preceding discussion applies only to the Mo sublattice. When the same set of Cl positions are included in the calculations, the diffraction for the two structures related by the Mo occupancy condition described above is similar but not identical. The freedom of the Cl atoms to move during the structural refinement allows them to compensate for this difference in the full structures. Table I shows how the Cl position changes along with the Mo occupancies. The resulting Mo−Cl interatomic distances for the two structures are plotted in Figure 2. All of the bond distances are reasonable considering the occupancies, and so this information does not help distinguish between the two structures. The variation is nearly linear for the three sites in both structures, and extrapolates to 2.393 Å for full occupancy. This distance corresponds to a bond valence sum of 3.7 for Mo[35,36], reasonably close to the expected value of 4. For comparison, the average Mo−Cl distance in $MoCl_3$ is 2.416 Å[26] and 2.36 Å in $MoCl_5$[37]. Thus, the Mo-Cl distances do not provide any information that might help reveal a preference between structures A and B. It is likely

TABLE I. Crystal data and structural refinement results for $MoCl_4$. Both structures have Mo1 at (0, 0, 1/4), Mo2 at (2/3, 1/3, 1/4), and Mo3 at (1/3, 2/3, 1/4). Equivalent isotropic displacement parameters U_{eq} are defined as one third of the trace of the orthogonalized U_{ij} tensor and given in units of $Å^2$. Statistical uncertainties estimated by the data analysis programs are included in parentheses.

Empirical formula	$MoCl_4$	
Temperature	175 K	
Wavelength	0.71073 Å	
Crystal system	Trigonal	
Space group, Z	$P\overline{3}1c$, 3	
a	6.0411(16) Å	
c	11.636(3) Å	
Volume	367.8(2) $Å^3$	
Density (calculated)	3.220 g/cm^3	
Crystal size	0.17 x 0.13 x 0.02 mm^3	
Refl. collected	3267	
R_{int}	0.0364	
Data / parameters	311 / 19	
	Structure A	Structure B
Goodness-of-fit on F^2	1.068	1.055
R_1 [$I > 2\sigma(I)$]	0.0368	0.0368
wR_2[$I > 2\sigma(I)$]	0.0852	0.0842
R_1 (all data)	0.0481	0.0481
wR_2 (all data)	0.0981	0.0973
Largest diff. peak	0.858 e/$Å^3$	0.727 e/$Å^3$
Largest diff. hole	-1.006 e/$Å^3$	-0.680 e/$Å^3$
x Cl	0.6743(2)	0.6589(2)
y Cl	0.0086(2)	-0.0087(2)
z Cl	0.1316(1)	0.1316(1)
occupancy Mo1	0.684(5)	0.324(5)
occupancy Mo2	0.756(6)	0.252(5)
occupancy Mo3	0.072(5)	0.936(7)
U_{eq} Cl	0.030(1)	0.030(1)
U_{eq} Mo1	0.031(1)	0.028(1)
U_{eq} Mo2	0.030(2)	0.030(1)
U_{eq} Mo3	0.023(4)	0.031(1)

that a more local probe of the structure, like pair distribution function analysis, will be required to distinguish the models.

A powder x-ray diffractogram from the bulk of the reaction product is shown in Figure 1a. The broad feature near 18 degrees is from the sample holder. The data is shown on a square root scale to compensate for texture in the powder sample. The curve through the data points represents a Lebail fit, showing that the data is described well by the unit cell and symmetry determined from the single crystal diffraction data. Texture and degradation of the powder sample over time precluded Rietveld analysis. Room temperature lattice parameters of $a = 6.0665(5)$Å and $c = 11.668(1)$ Å are determined from the powder diffraction data. As expected these are somewhat larger than those determined by single crystal x-ray diffraction at 175 K (Table I).

B. Magnetic behavior

As noted in the Introduction, the magnetic behavior of $MoCl_4$ has not been extensively studied. Several values

TABLE II. $MoCl_4$. Anisotropic displacement parameters ($10^{-3}Å^2$) determined by single crystal x-ray diffraction at 175 K. The anisotropic displacement factor exponent takes the form: $-2\pi^2[h^2a^{*2}U_{11} + ... + 2hka^*b^*U_{12}]$

	U_{11}	U_{22}	U_{33}	U_{23}	U_{13}	U_{12}
Structure A						
Mo1	37(1)	37(1)	19(1)	0	0	19(1)
Mo2	36(1)	36(1)	18(1)	0	0	18(1)
Mo3	33(6)	33(6)	3(5)	0	0	17(3)
Cl1	30(1)	30(1)	29(1)	-5(1)	-4(1)	13(1)
Structure B						
Mo1	35(1)	35(1)	15(1)	0	0	18(1)
Mo2	37(2)	37(2)	16(2)	0	0	19(1)
Mo3	37(1)	37(1)	19(1)	0	0	18(1)
Cl1	31(1)	31(1)	29(1)	5(1)	4(1)	15(1)

TABLE III. Curie-Weiss fit parameters for $MoCl_4$.

sample	μ_{eff} (μ_B/Mo)	θ (K)
H⊥c	2.23	-27
H‖c	2.26	-35
poly. S1	2.15	-25
poly. S2	2.24	-26

of magnetic susceptibility reported near room temperature, 195 K, and 90 K were tabulated in Ref. 27 from which an effective moment of 2.31 to 2.54 μ_B and a Weiss temperature of -37 to -39 K were determined[38–40]. In the present work, measurement temperatures are extended down to 2 K on single crystals and polycrystalline material, and isothermal magnetization curves and ac magnetization data are reported. The results are summarized in Figures 3 and 4. Data are shown for two crystals, one with the measurement field aligned in the hexagonal plane (H⊥c) and one with the field out of the plane (H‖c), and two polycrystalline samples labeled S1 and S2 consisting of multiple small crystallites collected from the bulk growth products.

The magnetic susceptibility (M/H) measured in a 10 kOe field is shown in Figure 3a and 3d. Curie-Weiss fits for data above 75 K are shown in Table III, and are in reasonable agreement with the previous analysis[27]. The effective moments are smaller than expected for spin-only tetravalent Mo (S = 1, $\mu_{eff} = 2.83\ \mu_B$), and the Weiss temperatures indicate moderate antiferromagnetic interactions, with some anisotropy apparent in the single crystal samples. The nearest Mo−Mo distance is 3.5 Å, and the Mo−Cl interactions are expected to be strongly ionic, so covalency is not expected to play a significant role in reducing the magnetic moment. The reduced effective moment is perhaps most likely due to an antialigned orbital contribution, which could be expected with two singly occupied t_{2g} orbitals and spin-orbit coupling.

The insets of Figure 3a and 3d show the deviation from the high temperature Curie-Weiss behavior at lower temperatures, which is seen below 50−75 K, and consistent with the onset of some antiferromagneic correlations. An anomaly is also observed below 10 K in this data. The low temperature behavior is shown in more detail in Figure 3b and 3e. A clear magnetic anomaly is observed near 5 K, corresponding to a kink in

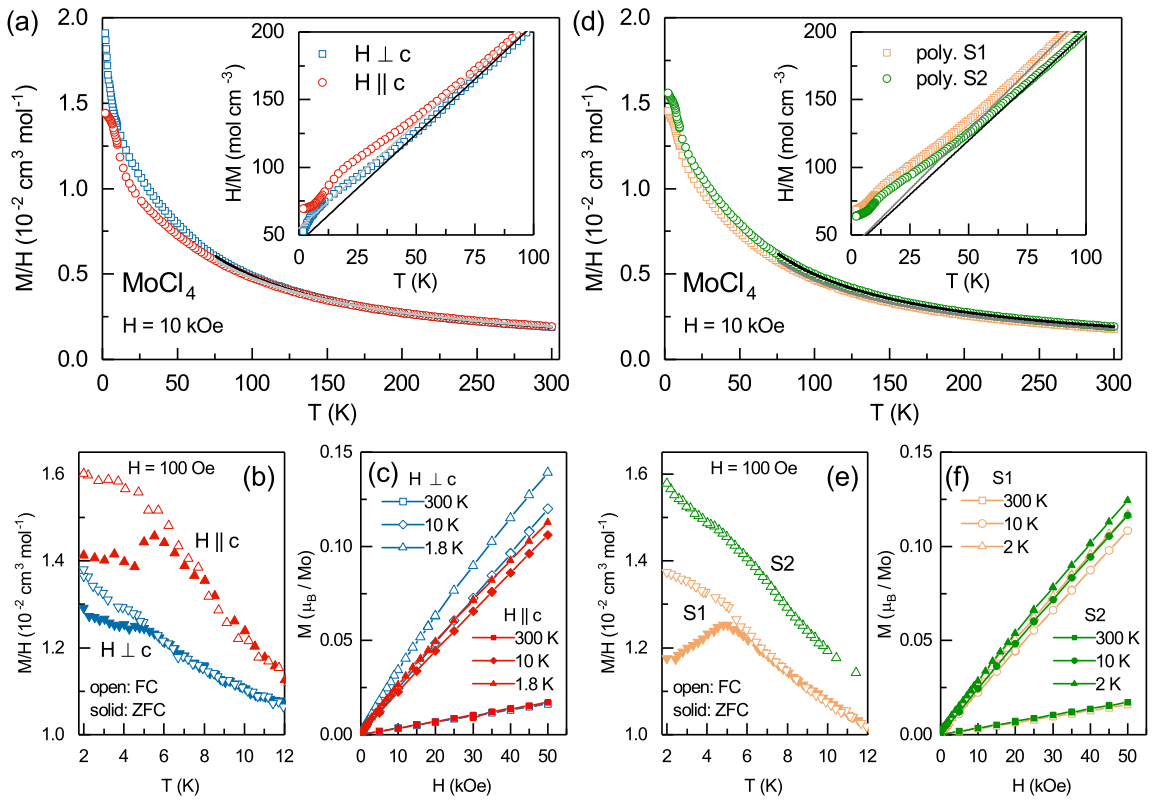

FIG. 3. Magnetic behavior of $MoCl_4$. Anisotropic data from single crystals are shown in (a-c). Data from polycrystalline samples S1 and S2 collected from two different growths are shown in (d-f). (a,d) Temperature dependence of the magnetic susceptibility (M/H) measured in a 10 kOe applied field with Curie-Weiss fits to data above 75 K, and inverse susceptibility with the linear Curie-Weiss behavior extended to low temperature shown in the insets. (b,e) Low temperature magnetic susceptibility collected in a 100 Oe applied field during field-cooled (FC) and zero field cooled (ZFC) measurements. (c,f) Isothermal magnetization curves measured at the indicated temperatures.

the susceptibility and a divergence between field cooled (FC) and zero field cooled (ZFC) data. Anisotropy is seen at the lowest temperatures, where the moment along the c-axis becomes nearly temperature independent while the moment in the plane increases upon cooling. This suggests antiferromagnetism with moments that prefer to lie along the c-axis.

Isothermal magnetization curves are shown in Figure 3c and 3f. They are essentially linear at all temperatures, again consistent with antiferromagnetism. Small remanent magnetizations are observed below the transition. This, along with the FC-ZFC divergence in M vs T suggest the magnetic ground state could be either antiferromagnetically ordered with a very small canted moment or glassy. The later is deemed more likely considering the lack of strong anisotropy in the magnetic data and the heavily disordered Mo sublattice.

To investigate the dynamics of the magnetism, ac measurements and time dependent dc magnetic measurements were performed. Results from one of the polycrystalline samples are shown in Figure 4. Near and below the temperature at which the anomaly was noted in the dc magnetic susceptibility, the real part of the ac susceptibility (χ') develops an enhanced frequency dependence (Figure 4a) and the imaginary part (χ") displays a peak (Figure 4b). The frequency dependence of the peak in χ' is shown in more detail in Figure 4c, and behavior typical of a spin glass is observed, with the maximum moving to higher temperature and smaller magnitude as the frequency is increased. The locations of the maxima are estimated from the second order polynomial fits to the data shown in the figure. The imaginary part of the magnetization (Figure 4b) was near the detection limit of our apparatus (10^{-7} emu) resulting in some scatter in the data, especially at the lowest frequencies, but a general increase in amplitude with increasing frequency is noted, as expected for a spin-glass.

To further confirm the slow dynamics of the magnetization in β-$MoCl_4$, the dc magnetic moment was measured as a function of time after cooling in a 10 kOe applied field and then decreasing the field zero. The results are shown in Figure 4d. The decay of the thermo-remanant magnetization was measured after cooling the sample in a 10 kOe applied field from 20 K to the measurement temperature and then turning the applied field to zero. The change in the dc magnetization (ΔM_{dc}) with time is plotted and fit with a stretched exponential function of the form $\Delta M_{dc}(t) = M_0 + A\exp(-(t/\tau)^{\beta})$. This function describes the data reasonably well. The fitted values of τ for data at 2, 3, and 4 K were 28, 20, and 15 min,

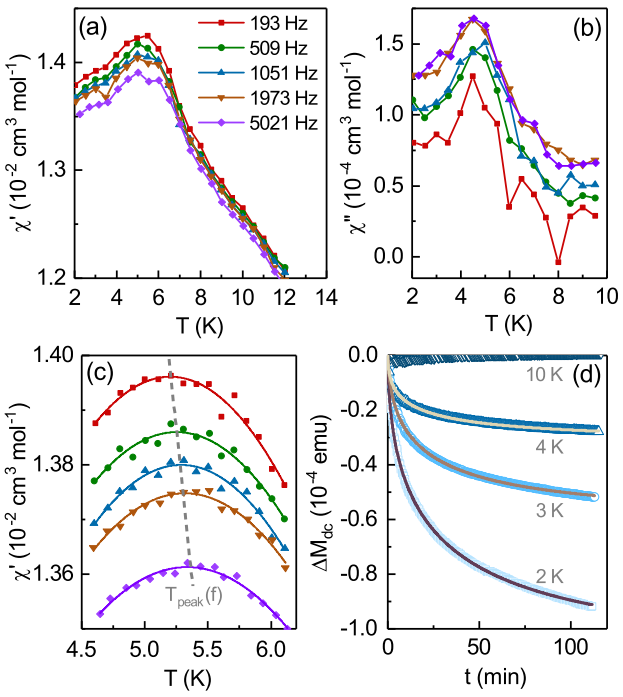

FIG. 4. Glassy dynamics in β-$MoCl_4$. (a) Real part of the ac magnetic susceptibility measured in zero applied dc field with an ac excitation of 13 Oe at the indicated frequencies. (b) Imaginary part of the ac magnetic susceptibility. (c) Frequency dependence of the temperature at which the maximum of χ' occurs. (d) Time dependent change in the dc magnetization after cooling to the indicated temperature in a 10 kOe field and then reducing the field to zero, with stretched-exponential fits described in the text.

respectively, and β values ranged from 0.42 to 0.48. The relaxation of the thermo-remanent magnetization in the glassy state is slow, and becomes more rapid as the glass transition temperature is approached from below. Negligible time dependence of the magnetization was seen at 10 K.

As noted above, the glasslike dynamics likely originate in the heavily disordered nature of the Mo layers in β-$MoCl_4$. It appears that spin glasses are rare among layered transition metal halides, though such behavior has been reported in a graphite intercalation compound with $FeCl_3$[41,42]. Among other van der Waals layered materials, spin glasses have been reported for certain compositions in the chemically disordered chalcogenides $Mn_{1-x}Fe_xPS_3$ and $Fe_{1-x}Ni_xPS_3$[43–45].

IV. SUMMARY AND CONCLUSIONS

The crystallographic and magnetic properties of the van der Waals layered $4d$ transition metal compound β-$MoCl_4$ have been revisited and revised. A structure with more complex vacancy distribution than previously reported is found, with some occupation of all of the sites within the triangular transition metal net. Interesting, two models with different vacancy orderings describe the experimental data equally well, and this seems to be a property of the three interpenetrating triangular sublattices that define the close packed layer. The magnetic properties are consistent with an orbital contribution to the total paramagnetic effective moment, and net antiferromagnetic interactions. Low temperature ac and dc magnetization measurements reveal the hallmarks of a spin-glass-like state, with ZFC-FC divergence, frequency dependent magnetic susceptibility, and a slow decay of thermo-remanent magnetization. Such behavior may be expected for this highly disordered and antiferromagnetic Mo lattice.

Development of cleavable magnetic materials is important in pushing forward our understanding of 2D physics and the functionality of heterostructured devices. While the main interest is in materials with long range magnetic order and associated phase transitions, spin glass materials with metastable, local magnetic configurations and associated temporal relaxation could make interesting additions to the menu of magnetic materials for van der Waals heterostructures.

ACKNOWLEDGEMENTS

Research supported by the U. S. Department of Energy, Office of Science, Basic Energy Sciences, Materials Sciences and Engineering Division. The authors thank Andrew F. May and Jiaqiang Yan for helpful discussions throughout the course of this work, and Radu Custelcean for use of and assistance with the single crystal x-ray diffractometer.

* McGuireMA@ornl.gov

[1] A. K. Geim and I. V. Geigorieva, Nature **499**, 419 (2013).
[2] M. A. McGuire, H. Dixit, V. R. Cooper, and B. C. Sales, Chem. Mater. **27**, 612 (2015).
[3] B. Huang, G. Clark, E. Navarro-Moratalla, D. R. Klein, R. Cheng, K. L. Seyler, D. Zhong, E. Schmidgall, M. A. McGuire, D. H. Cobden, W. Yao, D. Xiao, P. Jarillo-Herrero, and X. Xu, Nature **546**, 270 (2017).
[4] D. Zhong, K. L. Seyler, X. Linpeng, R. Cheng, N. Sivadas, B. Huang, E. Schmidgall, T. Taniguchi, K. Watanabe, M. A. McGuire, W. Yao, D. Xiao, K.-M. C. Fu, and X. Xu, Science Advances **3**, e1603113 (2017).

[5] T. Song, X. Cai, M. W.-Y. Tu, X. Zhang, B. Huang, N. P. Wilson, K. L. Seyler, L. Zhu, T. Taniguchi, K. Watanabe, *et al.*, Science , eaar4851 (2018).
[6] V. Carteaux, D. Brunet, G. Ouvrard, and G. André, J. Phys.: Condens. Matter **7**, 69 (1995).
[7] S. Lebègue, T. Björkman, M. Klintenberg, R. M. Nieminen, and O. Eriksson, Phys. Rev. X **3**, 031002 (2013).
[8] X. Li and J. Yang, J. Mater. Chem. C **2**, 7071 (2014).
[9] C. Gong, L. Li, Z. Li, H. Ji, A. Stern, Y. Xia, T. Cao, W. Bao, C. Wang, Y. Wang, *et al.*, Nature **546**, 265 (2017).
[10] B. Chen, J. Yang, H. Wang, M. Imai, H. Ohta, C. Michioka, K. Yoshimura, and M. Fang, Journal of the Physical Society of Japan **82**, 124711 (2013).
[11] A. F. May, S. Calder, C. Cantoni, H. Cao, and M. A. McGuire, Phys. Rev. B **93**, 014411 (2016).
[12] C. Tan, J. Lee, S.-G. Jung, T. Park, S. Albarakati, J. Partridge, M. R. Field, D. G. McCulloch, L. Wang, and C. Lee, Nature communications **9**, 1554 (2018).
[13] Z. Fei, B. Huang, P. Malinowski, W. Wang, T. Song, J. Sanchez, W. Yao, D. Xiao, X. Zhu, A. May, W. Wu, D. Cobden, J.-H. Chu, and X. Xu, arXiv preprint arXiv:1803.02559 (2018).
[14] Y. Singh and P. Gegenwart, Physical Review B **82**, 064412 (2010).
[15] Y. Singh, S. Manni, J. Reuther, T. Berlijn, R. Thomale, W. Ku, S. Trebst, and P. Gegenwart, Physical review letters **108**, 127203 (2012).
[16] B. J. Kim, H. Jin, S. J. Moon, J.-Y. Kim, B.-G. Park, C. S. Leem, J. Yu, T. W. Noh, C. Kim, S.-J. Oh, J.-H. Park, V. Durairaj, G. Cao, and E. Rotenberg, Phys. Rev. Lett. **101**, 076402 (2008).
[17] K. Plumb, J. Clancy, L. Sandilands, V. V. Shankar, Y. Hu, K. Burch, H.-Y. Kee, and Y.-J. Kim, Physical Review B **90**, 041112 (2014).
[18] A. Banerjee, J. Yan, J. Knolle, C. A. Bridges, M. B. Stone, M. D. Lumsden, D. G. Mandrus, D. A. Tennant, R. Moessner, and S. E. Nagler, Science **356**, 1055 (2017).
[19] C. I. Hiley, D. O. Scanlon, A. A. Sokol, S. M. Woodley, A. M. Ganose, S. Sangiao, J. M. De Teresa, P. Manuel, D. D. Khalyavin, M. Walker, M. R. Lees, and R. I. Walton, Phys. Rev. B **92**, 104413 (2015).
[20] W. Tian, C. Svoboda, M. Ochi, M. Matsuda, H. B. Cao, J.-G. Cheng, B. C. Sales, D. G. Mandrus, R. Arita, N. Trivedi, and J.-Q. Yan, Phys. Rev. B **92**, 100404 (2015).
[21] X.-L. Sheng and B. K. Nikolić, Phys. Rev. B **95**, 201402 (2017).
[22] M. A. McGuire, Crystals **7**, 121 (2017).
[23] M. K. Wilkinson, E. O. Wollan, H. R. Child, and J. W. Cable, Phys. Rev. **121**, 74 (1961).
[24] E. O. Wollan, H. R. Child, W. C. Koehler, and M. K. Wilkinson, Phys. Rev. **112**, 1132 (1958).
[25] W. N. Hansen and M. Griffel, J. Chem. Phys. **28**, 902 (1958).
[26] M. A. McGuire, J. Yan, P. Lampen-Kelley, A. F. May, V. R. Cooper, L. Lindsay, A. Puretzky, L. Liang, S. KC, E. Cakmak, S. Calder, and B. C. Sales, Phys. Rev. Mater. **1**, 064001 (2017).
[27] H. Schäfer, H. G. von Schnering, J. V. Tillack, F. Kuhnen, H. Wörle, and H. Baumann, Z. Anorg. Allgem. Chem. **353**, 281 (1967).
[28] H. Hillebrecht, P. J. Schmidt, H. W. Rotter, G. Thiele, P. Zönnchen, H. Bengel, H. J. Cantow, S. N. Magonov, and M. H. Whangbo, J. Alloys. Compd. **246**, 70 (1997).
[29] D. Kepert and R. Mandyczewsky, Inorg. Chem. **7**, 2091 (1968).
[30] E. A. Pisarev, D. V. Drobot, and I. V. Makachuk, Russ. J. Inorg. Chem. **27**, 10 (1982).
[31] D. M. Korotin, V. I. Anisimov, and S. V. Streltsov, Sci. Rep. **6**, 25831 (2016).
[32] U. Müller, Angew. Chem. Int. Ed. Engl. **20**, 692 (1981).
[33] G. M. Sheldrick, Acta Cryst. A **64**, 112 (2008).
[34] L. J. Farrugia, J. Appl. Cryst. **45**, 849 (2012).
[35] I. D. Brown and D. Altermatt, Acta Crystallographica Section B: Structural Science **41**, 244 (1985).
[36] I. D. Brown, "Accumulated table of bond valence parameters," `https://www.iucr.org/__data/assets/file/0007/126574/bvparm2016.cif`.
[37] J. Beck and F. Wolf, Acta. Crystallogr. B **53**, 895 (1997).
[38] B. T. Tjabbes, Proc. Kon. Akad. Wetensch. Amsterdam **35**, 693 (1932).
[39] W. Klemm and H. Steinberg, Z. Anorg. Allg. Chem. **227**, 193 (1936).
[40] M. L. Larson and F. W. Moore, Inorg. Chem. **3**, 285 (1964).
[41] K. Miyoshi, M. Hagiwara, M. Matsuura, T. Abe, and Y. Mizutani, Physica B: Condensed Matter **237**, 190 (1997).
[42] M. Suzuki and I. S. Suzuki, Phys. Rev. B **58**, 371 (1998).
[43] Y. Takano, A. Arai, Y. Takahashi, K. Takase, and K. Sekizawa, J. Appl. Phys. **93**, 8197 (2003).
[44] T. Masubuchi, H. Hoya, T. Watanabe, Y. Takahashi, S. Ban, N. Ohkubo, K. Takase, and Y. Takano, J. Alloys Compd. **460**, 668 (2008).
[45] D. J. Goossens, S. Brazier-Hollins, D. R. James, W. D. Hutchinson, and J. R. Hester, J. Magn. Magn. Mater. **334**, 82 (2013).